High-Spin Iron(VI), Low-Spin Ruthenium(VI), and Magnetically Bistable Osmium(VI) in Molecular Group 8 Nitrido Trifluorides NMF3

Tony Stüker,[a] Xiya Xia,[a] Helmut Beckers,[a] and Sebastian Riedel*[a]

Abstract: Pseudo-tetrahedral nitrido trifluorides $N\equiv MF_3$ (M = Fe, Ru, Os) and square pyramidal nitrido tetrafluorides $N\equiv MF_4$ (M = Ru, Os) were formed by free-metal-atom reactions with NF_3 and subsequently isolated in solid neon at 5 K. Their IR spectra were recorded and analyzed aided by quantum-chemical calculations. For a d^2 electron configuration of the $N\equiv MF_3$ compounds in C_{3v} symmetry, Hund's rule predict a high-spin $^3A_2$ ground state with two parallel spin electrons and two degenerate metal $d(\delta)$-orbitals. The corresponding high-spin $^3A_2$ ground state was, however, only found for $N\equiv FeF_3$, the first experimentally verified neutral nitrido Fe^{VI} species. The valence-isoelectronic $N\equiv RuF_3$ and $N\equiv OsF_3$ adopt different angular distorted singlet structures. For $N\equiv RuF_3$, the triplet $^3A_2$ state is only 5 kJ mol^{-1} higher in energy than the singlet $^1A'$ ground state, and the magnetically bistable molecular $N\equiv OsF_3$ with two distorted near degenerate $^1A'$ and $^3A''$ electronic states were experimentally detected at 5 K in solid neon.

Introduction

The group 8 transition metals have eight electrons in their valence shell, but in addition to the well-known strong oxidizers RuO_4 and OsO_4, only Os has a variety of different complexes in oxidation state VIII.[1] While the oxidation state VI is abundant for ruthenium and osmium, the complex anion $[FeO_4]^{2-}$ was the only known Fe^{VI} compound for a long time.[2] In 2007 the neutral, dioxo Fe^{VI} peroxide $O_2Fe(\eta^2\text{-}O_2)$ was reported to be formed from molecular FeO_2 and O_2 under cryogenic conditions.[3] Tetrahedral $Fe^{VIII}O_4$ was shown to be metastable with respect to $O_2Fe^{VI}(\eta^2\text{-}O_2)$ in the gas phase,[4] and the oxidation state VII is so far the highest oxidation state of iron observed experimentally for the tetrahedral tetroxide anion FeO_4^-.[5] In addition to oxygen, nitrogen ligands are also able to stabilize high oxidation states of iron. Such terminal iron-nitrido complexes have already been the subject of several up-to-date reviews.[6] We restrict ourselves to some representative examples such as the square-pyramidal $[(TPP)Fe^VN]$ (TPP^{2-} = tetraphenylporphyrinate dianion), characterized by Raman spectroscopy,[7] the tetragonal nitrido Fe^{VI} dication $[(Me_3cyac)FeN]^{2+}$ ($[Me_3cyac]^-$ = N,N,N-tri-methyl-1,4,8,11-tetraazacyclotetra-decane-1-acetate), confirmed by Mössbauer and X-ray spectroscopy,[8] the pseudo-tetrahedral $[(PhB(PCH_2PiPr_2)_3)Fe^{IV}N]$ ($PhB(PCH_2PiPr_2)_3$ = tris(diisopropylphosphinophenyl)borane),[9] and, very recently, the crystal structure of a thermally stable four-coordinate Fe^{VI} bis(imido) cation, $[(H_2B(MesIm)_2)Fe(=NMes)_2]^+$ ($[H_2B[MesIm]_2]^-$ = dihydrobis-[1-(2,4,6-trimethylphenyl)imidazol-2-ylidene]borato).[10]
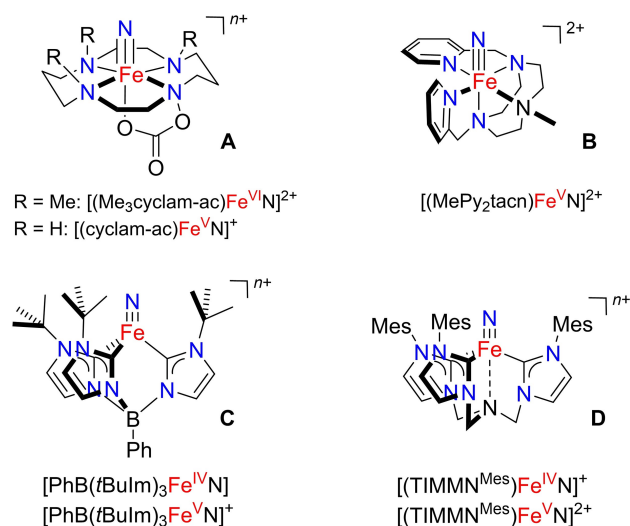
Nitrido iron complexes play an important role in a number of chemical and biological processes, for example in the catalytic cycle of cytochrome P450,[11] in the FeMo cofactor of the nitrogenase enzyme[6a] and in the Haber–Bosch process.[12] In analogy to the active iron surface nitride in the Haber–Bosch process, ammonia synthesis has also successfully achieved under mild conditions using the ruthenium pincer nitrido complex $[(PNP)RuN]$ (PNP^- = $[N(CH_2CH_2P^tBu_2)_2)]^-$).[13] Quite recently osmium(VI) nitrides have emerged as a new class of potential anticancer and antitumor agents.[14] Examples include $[(bipy)Cl_3Os^{VI}N]$[15] ($bipy$ = 2,2'-bipyridine)[16] and $[(sap)(py)ClOs^{VI}N]$ (sap = deprotonated N-salicylidene-2-aminophenol).[17] The wide field of possible applications of group 8 nitrido complexes underline the importance of a deeper understanding of the properties of this class of compounds. Especially the nitrido metal–ligand multiple bond and the valency of the metal are key factors for the reactivity and structure of these compounds.

In particular, there has been a tremendous progress in the synthesis and the chemistry of molecular Fe^{IV} and Fe^V nitrido compounds in the recent years that have been described in detail in several review articles.[6] They are supported by sterically encumbered macrocyclic or chelating ligands involving nitrogen or N-heterocyclic carbene donors based on, for example porphyrin or nitrogen- and boron-anchored tri- and tetrapodal chelates to protect the reactive $Fe\equiv N$ moiety (see Scheme 1 for representative examples). The most common route to these nitrido compounds is the photolysis of an iron azido precursor and concomitant N_2 evolution, whereby the

[a] T. Stüker, X. Xia, Dr. H. Beckers, Prof. S. Riedel
Institut für Chemie und Biochemie, Anorganische Chemie
Freie Universität Berlin
Fabeckstr. 34/36, 14195 Berlin (Germany)
E-mail: s.riedel@fu-berlin.de

Chemistry–A European Journal

Full Paper
doi.org/10.1002/chem.202101404

Chemistry Europe
European Chemical
Societies Publishing

Scheme 1. Representative examples of ligand-supported tetragonal (**A**[8,22] and **B**[19d]) and trigonal (**C**[19a] and **D**[19b]) coordinated high-valent iron nitrido complexes.

one-electron oxidation of the Fe^{IV} nitrido complexes often represents an alternative route to Fe^V nitrido complexes.[6a,b]

The reactivity of these high-valent nitrido iron compounds in chemical transformations have been thoroughly explored,[6,18] their structures, and their electronic properties have been investigated in detail using a variety of experimental and quantum mechanical methods.[19] While these studies contributed greatly to the understanding of the iron nitride bonding motif, our knowledge about the behavior, the nature, and bond-strengths of the $Fe\equiv N$ triple bond in high valent iron compounds upon iron oxidization is, however, still very limited and contradictory. Two questions arise here: *Is there a nitrido wall*[20] *from which the nitrido ligand gives up its innocent behavior,*[21] *and does the $Fe\equiv N$ bond become stronger and stronger through oxidation of the iron center?*

It should be emphasized that the known iron nitrido species can be divided into trigonal (pseudo-tetrahedral) and tetragonal (pseudo-octahedral) complexes (Scheme 1), since these two groups show different ligand field splitting of the Fe(3d) orbitals.[9,23] In a trigonal C_{3v} ligand field there are two purely $Fe\equiv N$ nonbonding e-type orbitals (d_{xy,x^2-y^2}), which allow the accommodation of up to four electrons energetically below the antibonding $Fe\equiv N$ orbitals.[6a,c,9,23] This results in a relatively strong $Fe\equiv N$ triple bonds, for example, low spin Fe^{IV} derivatives, for which very short experimental Fe–N distances (Table S1 in the Supporting Information) and Fe–N stretching vibrations at 1008–1034 cm^{-1} were found.[9,24]

Conversely, in the tetragonal C_{4v} ligand field there is only one purely nonbonding (d_{xy}) orbital with respect to the $Fe\equiv N$ bond energetically below the π^*-antibonding ($d_{xz,yz}$) MOs.[6a,c] A d-electron count larger than two results here in the occupation of $\pi^*(Fe\equiv N)$ orbitals, and, accordingly, Fe^{IV} (d^4) and Fe^V (d^3) nitrido complexes in tetragonal symmetry are generally thermally less stable and more reactive.[6b,18a,c] Note that the d^3 ground-state electron configuration of Fe^V nitrido complexes is

subject to a Jahn–Teller distortion.[19b,c] To overcome the thermal instability and high reactivity of such tetragonal Fe^V nitride complexes their $Fe\equiv N$ distances and stretching frequencies were obtained by a variety of spectroscopic methods either at cryogenic temperatures or at the gas phase (for representative examples, see Table S1). As expected, the experimental Fe–N distances for the two tetragonal complexes [Fe^V-(N)(MePy$_2$tacn)]$^{2+}$ (Scheme 1, 3d^4 configuration, Fe–N: 164(1) pm)[19d] and [Fe^V(N) (cyclam-ac)]$^+$ (Scheme 1, cyclam-ac = 1,4,8,11-tetraazacyclotetradecane-1-acetato, Fe–N: 161(1) pm),[22] estimated from extended X-ray absorption fine structure (EXAFS) analysis, were found to be longer than the Fe–N distance of the analogous Fe^{VI} dication [Fe^{VI}(N)(Me$_3$cyclam-ac)]$^{2+}$ (Scheme 1, 157(2) pm) with a singlet 3d^2 configuration.[8]

In contrast, the formal $Fe\equiv N$ bond order in trigonal Fe-nitrido complexes does not change by increasing the iron oxidation state from singlet Fe^{IV} to triplet Fe^{VI}, making predictions about the bond lengths less intuitive as other factors such as the geometry and the nature of the ligands come to the fore. X-ray structure analysis of the $Fe^{IV}N/Fe^VN$ derivatives of the two redox pairs [PhB(tBuIm)$_3$FeN]$^{0/+}$ (Scheme 1)[19a,24b] and [(TIMMN^{MES})FeN]$^{+/2+}$ (Scheme 1)[19b] show different trends. While the Fe–N length decreases slightly from 151.2(1) pm to 150.6(2) pm for the former, it increases from 151.3(3) pm to 152.9(1) pm for the latter. The different trend in these $Fe\equiv N$ distances during oxidation of Fe^{IV} to Fe^V was attributed to a possibly stronger interaction between the ligand N anchor with the more electrophilic Fe^V center in [Fe-(N)(TIMMN^{MES})]$^{2+}$ (Scheme 1).[19b] On the other hand, also coordinated solvent molecules can make it difficult to compare the $Fe\equiv N$ distances of different complexes, since this leads to shortened experimental $Fe\equiv N$ distances.[19e]

In this work, we describe the preparation of the molecular, neutral nitrido trifluorides NM^{VI}F$_3$ of the group 8 metals M = Fe, Ru, Os from IR laser ablated metal atoms and gaseous NF$_3$ and their IR-spectroscopic characterization under cryogenic conditions in a noble gas matrix. These trigonal nitrido trifluorides bear genuine $M\equiv N$ triple bonds, unsupported by sterically encumbered electron donor substituents with the innocent fluoride ligand. The $M\equiv N$ stretching vibration of theses derivatives is energetically sufficiently isolated from other fundamentals. Hence, it is considered to be a reliable experimental signature for M–N bond strength and M–N bond length in these nitrido complexes. This analysis overcomes the difficulties described above and also has the advantage that the experimental results can be supported and analyzed by reliable and accurate quantum mechanical calculations of these molecular, neutral compounds. Furthermore, this analysis enables a direct comparison of experimental $M\equiv N$ stretching frequencies of M = Fe^{VI} and its heavier group 8 congeners with those of the analogous nitrido trifluorides $N\equiv MF_3$ of group 6 (M = Cr, Mo, W)[25] and group 9 (Co, Rh, Ir)[26] transition metals which have been studied previously. To the best of our knowledge, $N\equiv Fe^{VI}F_3$ is the first experimentally verified neutral, nitrido iron(VI) complex. In addition, we have evidence for the formation of NM^{VII}F$_4$ (M = Ru, Os).

Chemistry–A European Journal

Full Paper
doi.org/10.1002/chem.202101404

Chemistry Europe
European Chemical
Societies Publishing

For an electronic metal d^2 configuration of these $N\equiv MF_3$ compounds in C_{3v} symmetry Hund's rule predict that two parallel spin electrons occupy the degenerate $M(d_{xy,x^2-y^2})$ orbitals of e-type symmetry resulting in a non-degenerate high-spin $^3A_2$ ground state. Although this $^3A_2$ state is not Jahn–Teller (JT) active, an electronic e^2 configuration can generally lead to a Jahn–Teller distorted ground state as a result of a strong pseudo-Jahn–Teller (PJT) mixing of two excited singlet electronic states.[27] This is because an electronic e^2 configuration in C_{3v} symmetry, in addition to the $^3A_2$ state, is generally associated with two electronic singlet states $^1A_1$ and ^1E. These electronic states are reminiscent of the well-known singlet excited states of molecular oxygen.[28]

It has been noted that the JT stabilization energy of the excited ^1E state is usually much weaker than the PJT stabilization resulting from mixing of the two excited $^1A_1$ and ^1E states. The stabilization energy of this PJT interaction can be so large that the lower of these excited states crosses the $^3A_2$ potential energy surfaces and become the distorted global minimum configuration.[27,31] We observed such a "hidden" PJT distortion for $N\equiv RuF_3$ and $N\equiv OsF_3$ but not for $NFe\equiv F_3$. Note that this distortion is also associated with a PJT-induced triplet-singlet spin crossover.[27a]

Results

Vibrational wavenumbers of group 8 nitrido trifluorides $NM^{VI}F_3$ and tetrafluorides $NM^{VII}F_4$

The IR spectra of the novel group 8 metal nitrido trifluorides, $N\equiv MF_3$ (M = Fe, Ru, Os) were recorded from the products obtained from laser-ablated free metal atoms with NF_3 seeded in a 1:1000 excess of neon after their deposition at 5 K on a gold-plated copper mirror (for experimental details see the Supporting Information). According to density functional theory calculations, the direct insertion of the metal atoms into an F–N bond of NF_3 to yield $F_2N–MF$, and the subsequent fluorine migration from nitrogen to the metal center to $FN\equiv MF_2$ is highly exothermic for all three metals (Figure 1, Table S2).

The rearrangement of the fluorimido complexes to the hexavalent nitrido trifluorides $N\equiv MF_3$ is found to be considerably exothermic for osmium ($-208\ \mathrm{kJ\,mol^{-1}}$), ruthenium ($-146\ \mathrm{kJ\,mol^{-1}}$), and iron ($-78\ \mathrm{kJ\,mol^{-1}}$) at the BP86/def2-QZVP[32] level of theory (details see the Supporting Information). Experimental IR spectra are shown from the deposits obtained in solid neon for the iron (Figures 2 and S1), ruthenium (Figures 3 and S2), and the osmium experiments (Figures 4 and S3), respectively. Experimental band positions are compared
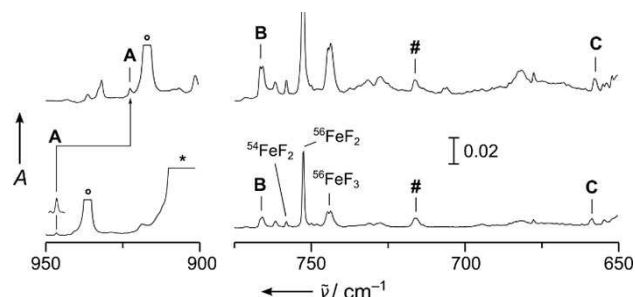
Figure 2. IR absorption spectra obtained from co-deposition of laser-ablated iron with 0.1% $^{14}NF_3$ (bottom) and 0.1% $^{15}NF_3$ (top) in solid Ne. Bands labeled with **A**, **B** and **C** are assigned to $NFeF_3$ (Table 1). Band **A** is enhanced by a factor of five. Known bands of binary iron fluorides[29] are labeled, and an unassigned band showing no $^{14/15}N$ isotopic shift is labeled with a hash mark. The bands associated with NF_2 and NF_3 are marked with circles and asterisks, respectively.[30] For more details, see Figure S1.
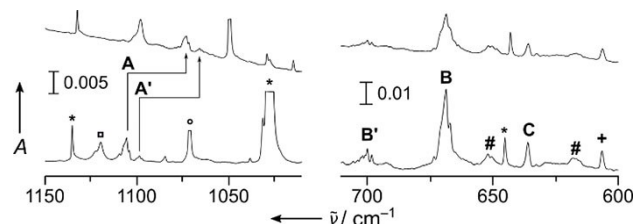
Figure 3. IR absorption spectra obtained from co-deposition of laser ablated ruthenium with 0.1% $^{14}NF_3$ (bottom), and $^{15}NF_3$ (top) in solid Ne, respectively. Bands labeled **A**–**C** are attributed to $NRuF_3$ and **A'** and **B'** are due to $NRuF_4$. Unknown bands are labeled by a pound and a plus sign, respectively. The bands associated with ^{14}NF, $^{14}NF_2$ and $^{14}NF_3$ are marked with squares, circles, and asterisks, respectively.[30] For more details, see Figure S2.
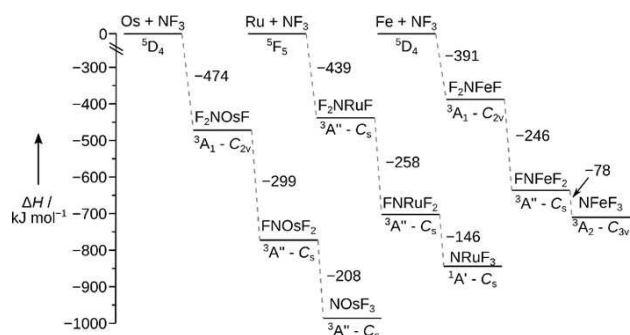

Figure 1. Stationary points on the reaction coordinate obtained at the BP86 level of theory for the formation of the nitrido metal complexes $N\equiv MF_3$ starting from the free metal atoms M and NF_3 ($C_{3v} - {}^1A_1$). See Table S2 for more details.

Figure 4. IR absorption spectra of laser ablated osmium co-deposited with 0.1% $^{14}NF_3$ in solid Ne (bottom), with 0.1% $^{15}NF_3$ in Ne (top). Bands labeled **A**–**D** are attributed to $NOsF_3$ ($^1A'$) and **A'**–**D'** to $NOsF_3$ ($^3A''$). The bands marked with a pentagram sign are binary osmium fluorides. The bands associated with NF, NF_2 and NF_3 are marked with squares, circles and asterisks, respectively.[30] For more details see Figure S3.

Chemistry–A European Journal
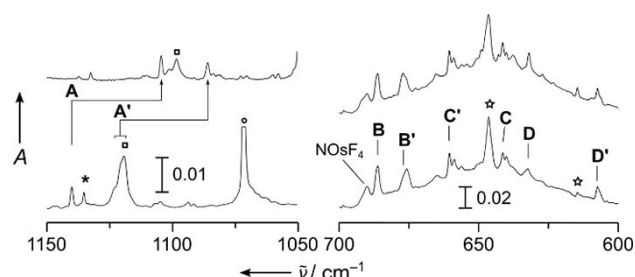
Full Paper
doi.org/10.1002/chem.202101404

Chemistry Europe
European Chemical
Societies Publishing

with predicted ones from quantum-chemical calculations in Tables 1 and S4 (for a detailed band assignment refer to the Supporting Information). The formation of molecular NFeF$_3$ (C_{3v}) is clearly proved by the assignment of all its stretching vibrations marked **A** (ν(NFe): 946.4 cm^{-1}), **B** (ν_{as}(FeF$_3$): 766.8 cm^{-1}), and **C** (ν_s(FeF$_3$): 658.8 cm^{-1}) in Figure 2 (Table 1). Bands at 743.6/744.7, 752.6 and 785.1 cm^{-1} were assigned to the known molecular binary iron fluorides ^{56}FeF$_3$, ^{56}FeF$_2$ and ^{54}FeF$_2$, respectively.[29] Their high intensity and the high yield of these binary fluorides compared to the NFeF$_3$ product bands indicate the lower stability of NFeF$_3$ under the harsh conditions of the laser ablation process. The spectra recorded in the ruthenium experiment (Figure 3), clearly revealed the presence of two different nitrido ruthenium complexes, finally assigned to NRuF$_3$ (C_s) and NRuF$_4$ (C_{4v}). The characteristic Ru≡N stretching bands of NRuF$_3$ (C_s) and NRuF$_4$ (C_{4v}) are labeled **A** (1105.4 cm^{-1}, NRuF$_3$) and **A'** (1098.5 cm^{-1}, NRuF$_4$) in Figure 3. The RuF$_3$ stretching modes of C_s symmetric NRuF$_3$ split into three modes. The strong antisymmetric F–Ru–F appears at 668.5 cm^{-1} (labeled **B** in Figure 3) and likely overlaps with the nearby weaker F'–Ru band. The symmetric F–Ru–F mode is attributed to the band labeled **C** in Figure 3 at 635.8 cm^{-1} (Table 1).

For NRuF$_4$ only the strongest RuF$_4$ stretching band, the degenerate e-type mode could safely be assigned to the band labeled **B'** in Figure 3 centered at 700.0 cm^{-1}.

In the spectra obtained from the reaction of osmium atoms with isotopic labeled ^{15}NF$_3$ two Os≡N stretching bands appeared at 1104.6 and 1086 cm^{-1}, which are labeled **A** and **A'**, respectively, in Figure 4, and which are finally assigned to different "spin-isomers" of NOsF$_3$ in near-degenerate singlet ^{1}A' and triplet ^{3}A'' electronic states (Table 1). In the ^{14}NF$_3$ experiment **A** is observed at 1140 cm^{-1} (Figure 4), while **A'** is overlapped by a stronger band due to the ^{14}NF radical at 1120.8 cm^{-1}.[30b] All three Os–F stretching bands of singlet NOsF$_3$ (^{1}A') are assigned (Table 1) and labeled **B** (ν_s(OsF$_2$): 686.0 cm^{-1}), **C** (ν(OsF'): 641.3 cm^{-1}), and **D** (ν_{as}(OsF$_2$): 632.3 cm^{-1}) in Figure 4, respectively. Bands labeled **B'**, **C'** and **D'** at 675.8 cm^{-1}, 660.5 cm^{-1} and 607.4 cm^{-1}, respectively, are assigned to the three Os–F stretching modes of triplet NOsF$_3$ (^{3}A'', Table 1). Finally, a band at 689.6 cm^{-1} in Figure 4 is tentatively assigned to the strongest vibrational mode of NOsF$_4$ (C_{4v}, Table 1). The tetrafluorides N≡MF$_4$ (M = Ru, Os) are likely formed by the exothermic addition of a fluorine atom to N≡MF$_3$ (Table S2).

Pseudo-Jahn–Teller distortion of molecular group 8 nitrido fluorides NM^{VI}F$_3$

The group 8 nitrido fluorides NM^{VI}F$_3$ adopt metal d^2 configurations, for which Hund's rule predicts a high-spin ^{3}A$_2$ ground state in an undistorted C_{3v} symmetry and two parallel spin electrons in the twofold degenerate e(d$_{xy,x^2-y^2}$)-orbital ($|e_\varepsilon\uparrow;e_\theta\uparrow\rangle$), labeled 9e for NFeF$_3$ in the Supporting Information Figure S6. Three e^2 terms (four states) can be formed, ^{3}A$_2$ ($|e_\varepsilon\uparrow;e_\theta\uparrow\rangle$), ^{1}A$_1$ ($\sqrt{1/2}$ [$|e_\varepsilon\uparrow;e_\varepsilon\downarrow\rangle + |e_\theta\uparrow;e_\theta\downarrow\rangle$]), ^{1}E$_\theta$ ($\sqrt{1/2}$ [$|e_\varepsilon\uparrow;e_\varepsilon\downarrow\rangle - |e_\theta\uparrow;e_\theta\downarrow\rangle$]) and ^{1}E$_\varepsilon$ ($\sqrt{1/2}$ [$|e_\theta\uparrow;e_\varepsilon\downarrow\rangle + |e_\theta\downarrow;e_\varepsilon\uparrow\rangle$]). Due to the nondegenerate nature and totally symmetric charge distribution of the ^{3}A$_2$ state no Jahn–Teller distortion is expected.[31] Other distributions of the electrons, as outlined above, result in configurations with lower spin and the absence of low-lying triplet excited states rule out obvious ground state pseudo-Jahn–Teller distortions.

Nevertheless, as shown in Figure 5 and in agreement with experimental vibrational assignments, all four NMF$_3$ species possess surprisingly different structures and the C_{3v} symmetric ground state was only verified for NFeF$_3$. In case of NRuF$_3$, extensive CCSD(T)/CBS calculations (Table S10) find the high symmetric ^{3}A$_2$ is just about 5 kJ mol^{-1} higher than the distorted ^{1}A' ground state. According to our experimental data, NOsF$_3$ features two quasi-degenerate, distorted structures in ^{1}A' and ^{3}A'' electronic states, separated by only $\Delta E_{T-S} = -1.3$ kJ mol^{-1} (CCSD(T)/CBS, Table S11).

To elucidate these findings, adiabatic potential energy surface (APES) scans were carried out using state-averaged complete active space self-consistent field calculations by distributing eight electrons in the eight molecular orbits formed by the metal (n-1)d and N(2p) orbitals (SA-CASSCF(8,8)) with subsequent NEVPT2 treatment to recover dynamic correlation. Shown in Figure 6a–c are cross sections along a distortion coordinate (D) that connects the two stationary points of the

Table 1. Calculated and experimental vibrational wavenumbers (ν(^{14}N) in cm^{-1}) and $^{14/15}$N isotopic shifts ($\Delta\nu$ in parentheses) for NFeF$_3$, NRuF$_3$, NRuF$_4$, NOsF$_3$ and NOsF$_4$.

Exp.[a]	CCSD (T)[b]	Assignment
NFeF$_3$ (C_{3v}, ^{3}A$_2$)[c]		
946.4 (−23.7)[d]	1028 (−26)[e,f]	NFe str., a$_1$
766.8/766.7 (0)	737 (0)[f]	FeF$_3$ str., e
658.8 (−1.1)	689 (−2)[f]	FeF$_3$ str., a$_1$
N^{102}RuF$_3$ (C_s, ^{1}A')[g]		
1105.4 (−32.7)	1085 (−32)	NRu str., a'
_[h]	682 (0)	F'-Ru str., a'
668.5 (0)	678 (0)	antisym. F–Ru-F str., a''
635.8 (0)	649 (0)	sym. F–Ru-F str., a'
N^{102}RuF$_4$ (C_{4v}, ^{2}B$_1$)[g]		
1098.5 (−32.5)	1080 (−32)	NRu str., a$_1$
700.1 (0)	711 (0)	RuF$_4$ stretch, e
_[h]	681 (0)	RuF$_4$ stretch, a$_1$
_[j]	598 (0)	RuF$_4$ stretch, b$_2$
NOsF$_3$ (C_s, ^{1}A')		
1140.1 (−35.5)	1152 (−36)	NOs str., a'
686.0/686.6 (0)	689 (0)	OsF$_2$ sym. str., a'
641.3/640.0 (0)	664 (0)	OsF' sym. str., a'
632.3 (0)	652 (0)	OsF$_2$ antisym. str., a''
NOsF$_3$ (C_s, ^{3}A'')		
1086.0 (−)[i]	1095 (−36)[i]	^{15}NOs str, a'
675.8/677.0	675 (0)	OsF$_2$ antisym. str., a''
660.5/658.9 (0)	668 (0)	OsF$_2$ sym. str., a'
607.4 (0.0)	614 (0)	OsF' sym. str., a'
NOsF$_4$ (C_{4v}, ^{2}B$_1$)		
_[k]	1145 (−36)	NOs str., a$_1$
_[k]	706 (0)	OsF$_4$ stretch, a$_1$
689.9 (0)	693 (0)	OsF$_4$ stretch, e
_[j]	635 (0)	OsF$_4$ stretch, b$_2$

[a] Neon matrix; matrix sites are separated by a slash. [b] Intensities from DFT calculations available in Table S4. [c] M06-L/def2-QZVP: 785 a$_1$ (−11) [12], 703 e (0) [200], 617 a$_1$ (−1) [40]. [d] $^{14/15}$N isotopic ratio: 1.0256. [e] $^{14/15}$N isotopic ratio: 1.0257. [f] NEVPT2/aug-cc-pwCVTZ-DK. [g] For the experimentally observed Ru isotope splitting see Tables S5–S7 and Figures S4 and S5). [h] Band is likely hidden by the stronger antisymmetric F–Ru–F stretching mode (a''). [i] ν(^{15}N–Os) in cm^{-1}, see text. [j] Not IR active. [k] Too weak or overlapped.

Chemistry–A European Journal

Full Paper
doi.org/10.1002/chem.202101404

Chemistry Europe
European Chemical
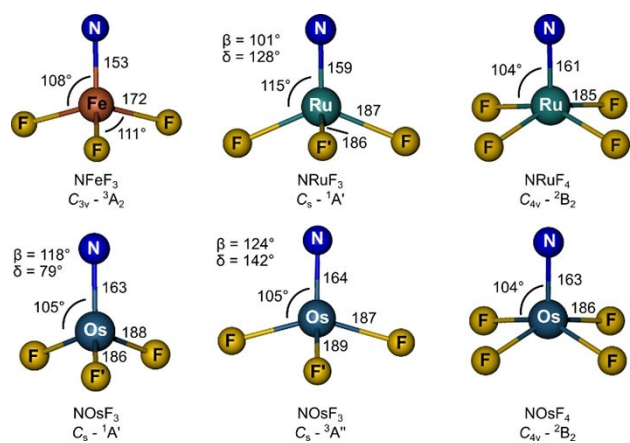Societies Publishing

Figure 5. Ground-state structures of NMF_3 and NMF_4 calculated at the CCSD (T)/aVTZ (M = Ru, Os, M: aVTZ-PP) and the NEVPT2/aVTZ-DK ($NFeF_3$, Fe: awCVTZ-DK) levels of theory. Bond lengths are given in pm and angles in degrees. β denotes the N–M–F' and δ the F–M–F angle for structures with C_s symmetry.

^{1}A' surface, at $D = -1$ and 1, respectively, via the high-symmetry C_{3v} stationary point at $D = 0$.

The distortions take place along one component of the lowest ($NFeF_3$, $NRuF_3$) or imaginary ($NOsF_3$) degenerate e normal mode in the high-symmetry C_{3v} configuration. Therefore, mainly bond angle distortions are involved, in particular the dihedral angle

F'–M–N–F (α, Figure S9), and the valence angles N–M–F' (β, Figure 5), and N–M–F (γ). The sign of the distortion D in Figure 6 indicates a widening (positive) or closing (negative) of α. Differences in these angles and in the three nonequivalent bond distances between two localized stationary points in C_s symmetry were divided into equal incremental steps and used as intermediate internal coordinates in the APES calculation for each step (Tables S14–S17). In the case of Figure 6d the distortion in the positive direction was carried out using the $NOsF_3$ ^{3}A'' minimum structure at $D = 1$. The graphs shown in Figure 6a–d represent the energies of the terms arising from the electronic e^2 configuration, as outlined above. They demonstrate the propensity of trigonal group 8 nitrido complexes in the oxidation state VI to be subject to a PJT distortion. Other trigonal systems displaying a (A + E) ⊗ e Pseudo-Jahn–Teller effect (PJTE) that is "hidden" in excited states (h-PJTE) have already been described.[27a,31] The condition for a distorted ground state minimum structure caused by the h-PTJE is that the PJT stabilization energy of an excited state (E_{PJT}) is larger than the energy gap Δ_0 between the ground state in the high-symmetry configuration and the PJT active excited state ($E_{PJT} > \Delta_0$, see Figure 6, a–c).[27a] The global minimum of the APES of $NFeF_3$ shown in Figure 6a is located at the high-symmetry point. The stationary points on the ^{1}A' (blue line) surface are a local minimum ($D = 1$) and a first-order saddle point ($D = -1$) without surface crossings in between. Consistent with the experimental vibrational data the global minimum is the high symmetry configuration. The h-PJTE in the ^{1}E state is not strong enough to distort the high-
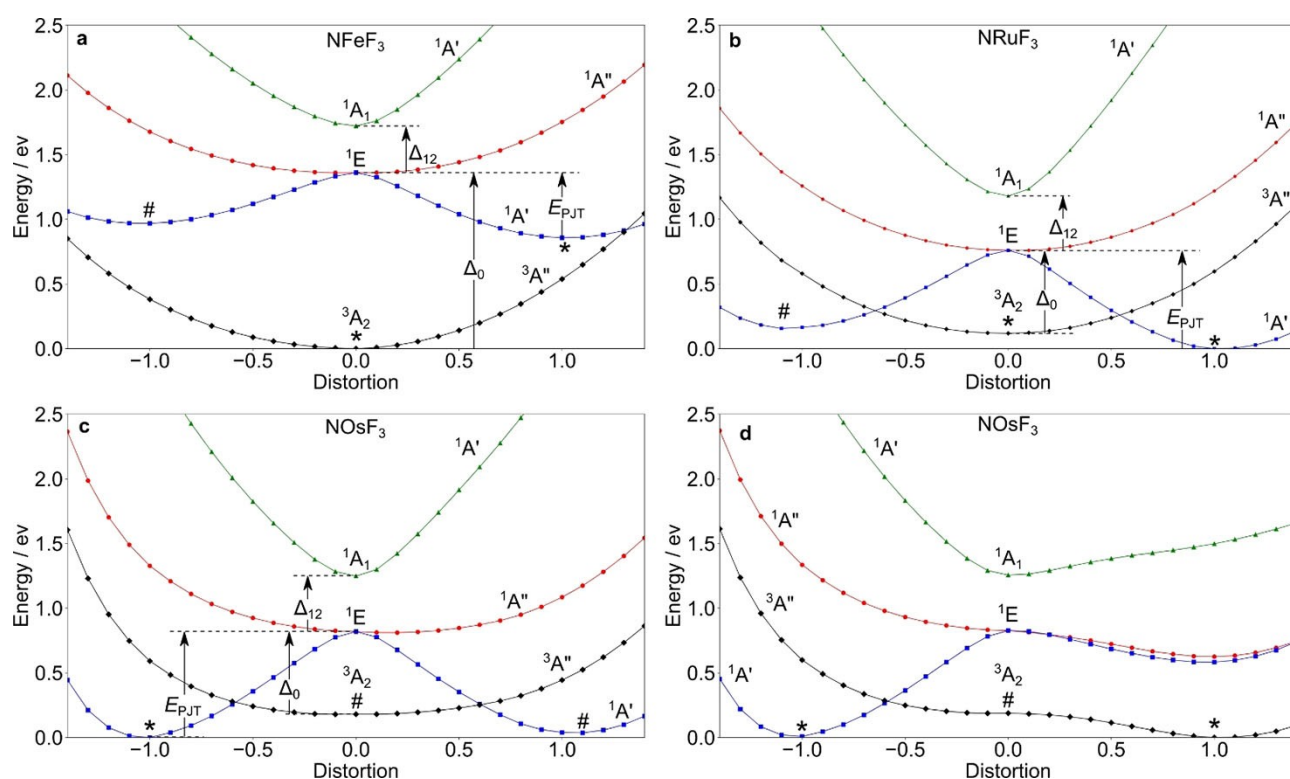

Figure 6. Cross section of the APES for the terms arising from the electronic e^2 configurations of a) $NFeF_3$, b) $NRuF_3$, c), d) $NOsF_3$ along the distortion coordinate (D) connecting stationary points located at $D = 1$, 0 and -1, respectively, on the ^{1}A' (blue line) and the ^{3}A$_2$ (^{3}A'', black line) surfaces. Minimum points are marked with an asterisk, and first-order saddle points with a hash mark. The PJT stabilization energy (E_{PJT}) of the lowest excited state, its excitation energy at C_{3v} symmetry (Δ_0), and the ^{1}E–^{1}A$_1$ energy gap (Δ_{12}) are indicated in (a)–(c).

Chemistry–A European Journal

Full Paper
doi.org/10.1002/chem.202101404

Chemistry
Europe
European Chemical
Societies Publishing

symmetry configuration. The PJT stabilization energy, E_{PJT}, is about 0.39 eV and smaller than the ^1E-$^3A_2$ energy gap $\Delta_0 = 1.36$ eV. The $^1A'$ minima, which features a ($|e_\theta\uparrow;e_\theta\downarrow\rangle$) electronic configuration, and the $^3A_2$ minima are separated by about 0.86 eV. The angular distortion from $D = -1$ to $D = 1$ at the $^1A'$ surface extends from about 101°–132° (α), 100°–120° (β), and 112°–104° (γ).

The cross section of the APES of NRuF$_3$ along the distortion coordinate from $D = 0$ to $D = 1$ illustrated in Figure 6b shows that one of the components of the ^1E term is stabilized by the strong PJT coupling with the excited $^1A_1$ state. It crosses the $^3A_2$ ground state of the undistorted high-symmetry configuration to produce the global minimum with a distorted structure. The triplet-singlet spin crossover is associated with an orbital disproportionation,[27a] because in the distorted structure the electrons are paired in one e_θ orbital ($|e_\theta\uparrow;e_\theta\downarrow\rangle$) instead of the symmetric distribution ($|e_\varepsilon\uparrow;e_\theta\uparrow\rangle$) in the undistorted configuration. Accordingly, we find that $E_{PJT} = 0.76$ eV is larger than $\Delta_0 = 0.64$ eV. The high-spin $^3A''$ state is higher in energy by only ~0.12 eV and it has an energy barrier of ~0.25 eV to the point of spin crossover with the low-spin $^1A'$ state.

Figures 6c and d exhibit four relevant low-lying stationary points on the $^1A'$ and $^3A''$ APES of NOsF$_3$. The h-PJTE in this case produces a minimum with a distorted $^1A'$ structure at $D = -1$ and accordingly, the orbital disproportionation and spin crossover leads to a ($|e_\varepsilon\uparrow; e_\varepsilon\downarrow\rangle$) configuration with $E_{PJT} = 0.82$ eV and $\Delta_0 = 0.60$ eV. Unlike the former two cases, the $^3A_2$ high-symmetry configuration of NOsF$_3$ does not represent a minimum point, but a first order saddle point. Following the ε component of the imaginary e mode in Figure 6d we find – in accordance with the CCSD(T)/CBS results – an energetically quasi-degenerate distorted $^3A''$ minimum that shows orbital disproportionation, but no spin crossover about 0.1 eV (or 0.7 kJ mol^{-1}) lower than the $^1A'$ state. The energy barrier of the spin crossover point is ~0.27 eV (CCSD(T)/VTZ-PP: 0.24 eV, Table S12), a significant barrier connecting both stationary points at the experimental cryogenic conditions. These findings support the observation of two different species in the experimental infrared spectra which correspond to species in different $^1A'$ and $^3A''$ electronic states. We did not analyze the source of the distortion of the high-spin minimum ($^3A''$). But, under the premise that PJTE is the only source for symmetry breaking of non-degenerate high-symmetry states,[27b,31] the source is most likely an interacting triplet ^3E excited state.

Discussion

All metal specific bands showing a $^{14/15}N$ isotopic shift were successfully assigned. Bands due to binary fluorides are always present in experiments using IR laser ablation of metals in the presence of molecular fluorides as precursors. They are likely formed by recombination of metal atoms and atomic fluorine radicals formed by thermal or photolytic decomposition of the fluoride precursor in the hot plasma plume region or by the decomposition of metal fluoride product molecules. However, the very strong NF$_3$ precursor bands and comparatively weak NF and NF$_2$ bands in all spectra suggest that the formation of the NMF$_3$

title product can be attributed to the reaction of M and NF$_3$. Lower nitrido fluorides NMF or NMF$_2$ could in principle also be formed through the cleavage of a metal-fluorine bond or by the reaction of metal atoms with NF or NF$_2$, but have so far not been identified.[25,26,30c,33] The addition of fluorine to NMF and NMF$_2$ to yield NMF$_3$ and also the formation of NMF$_4$ for M = Ru and Os are calculated to be exothermic (Table S2).

As shown here, all the trigonal NMF$_3$ species possess two equilibrium configurations with different spin multiplicities, while those of NRuF$_3$ and NOsF$_3$ are close in energy. Such a magnetic and structural PJT induced bistability may also be possible for ligand-stabilized trigonal nitrido d^2 metal complexes. Such compounds are of interest for molecular switching, especially when symmetry breaking is involved (as for NFeF$_3$ and NRuF$_3$).[34]

The different stationary structures that were obtained for the group 8 NMF$_3$ molecules shown in Figure 5 possess surprisingly different electronic configurations, as outlined above and summarized in Figure 7 (for molecular orbital plots, see Figures S6 and S8). The different $^1A'$ electronic ground states of NRuF$_3$ and NOsF$_3$ arise from the pairing of two unpaired electrons in different orbitals, which are associated with two different structural distortions. The HOMO of NRuF$_3$ ($^1A'$) is of a'' symmetry, which is consistent with a widening of the F–M–F angle, whereas the HOMO of NOsF$_3$ ($^1A'$) is of a' symmetry, which shows a reduction in the F–M–F angle bisected by the σ plane in C_s symmetry (Figure 5). The d^1 metal configuration for the heptavalent tetrafluorides NRu^{VII}F$_4$ and NOs^{VII}F$_4$ (C_{4v}) give rise to a $^2B_2$ electronic ground state (see Figure S7 for the singly occupied MO).

The effective bond orders[35] (EBOs) for NOsF$_3$, NRuF$_3$ and NFeF$_3$ are 2.8, 2.7 and 2.2, respectively, which in fact corresponds to triple bonds for all these M–N bonds. The computed M–N bond lengths for the novel nitrido compounds (153 pm (FeN), 159 pm (RuN), 163–164 pm (OsN), Figure 7) are close to our published triple bond additive covalent radii: 156 pm (FeN), 157 pm (RuN) and 163 pm (OsN),[36] and also the experimental N–M stretching frequencies (Table 1) support the presence of strong M≡N triple bonds in the novel hexavalent nitrido complexes NM^{VI}F$_3$. We note that the experimental ν(Fe≡N) frequency of NFe^{VI}F$_3$ of 946 cm^{-1} (Table 1) is not well reproduced by calculations at DFT or CCSD(T) levels (Table S3) and is also

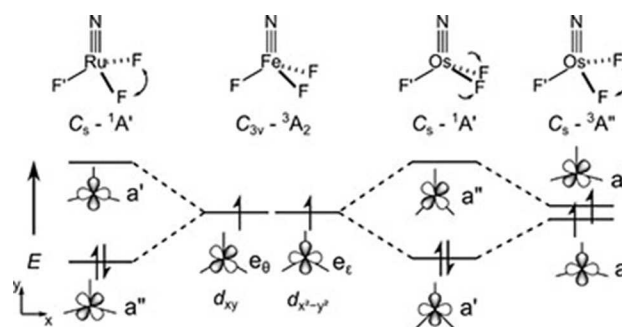**Figure 7.** Comparison of the different d^2 electron configurations of the NMF$_3$ species (M = Fe, Ru, Os). The metal centered a' and a''-MOs are dominantly M(d$_{x^2-y^2}$) and M(d$_{xy}$) atomic orbitals, respectively.

Chemistry–A European Journal

Full Paper
doi.org/10.1002/chem.202101404

Chemistry Europe
European Chemical
Societies Publishing

overestimated by the more sophisticated NEVPT2 multi-reference approach (ν(Fe≡N) = 1027 cm^{-1}, Table S3). On the other hand, its comparison with experimental Fe≡N stretching frequencies for pseudo-tetrahedral N^{IV}FeL$_3$ complexes, previously reported at 1008 ([Fe^{IV}(N)(TIMEN^{Mes})]$^+$),[24c] 1028 ([Fe^{IV}(N)(PhB(^{t}BuIm)$_3$)]),[24b] and 1034 cm^{-1} ([Fe^{IV}(N)-(PhB(CH$_2$P^{i}Pr$_2$)$_3$];[9] Table S1) suggests that an increase in the iron oxidation state beyond V does not necessarily lead to a stronger Fe≡N bond.

Table 2 shows experimental M–N stretching frequencies of molecular NMF$_3$ species formed by the reaction of NF$_3$ with laser-ablated transition metals. For the d^0 configurations of all group 4 and group 6 nitrido trifluorides the ideal pseudo-tetrahedral C_{3v} symmetric arrangement was experimentally verified, since there are no electrons in the nonbonding $e(d_{xy,x^2-y^2})$ orbitals that could cause distortions.[25,33] The e^3 configuration of NRhF$_3$ and NIrF$_3$ leads to Jahn–Teller distorted spin doublet ground states in C_s symmetry.[26] So far, no experimental data are available for the group 10 derivatives, and for the group 11 analogues only the initial metal insertion products F$_2$N–M^{II}F were detected after matrix deposition (irradiation of F$_2$NCuF led to rearrangement to metastable FN=CuF$_2$).[30c]

The M–N stretching normal mode of the terminally bond nitrogen ligands of the nitrido trifluorides can regarded to be a good approximation as an almost pure and uncoupled metal-nitrogen stretching mode that can be used as a measure of the M–N bond strength. The NM^{IV}F$_3$ derivatives of the group 4 metals possess a singly bonded triplet nitrene (^{3}N$^-$) ligand, since the ligand cannot oxidize the d^0 metal center any further. The two unpaired electrons in the N(2p) orbitals are reported to be involved in weak degenerate π bonding interactions for M=Ti ≫ Zr, Hf.[33] In contrast, the group 6, 8 and 9 NM^{VI}F$_3$ molecules show a N≡M triple bond with one σ and two π bonds to the terminal nitrido (N^{3-}) ligand. The strength and overlap of these bonds increases going down the groups likely due to an improved M(πd)–N(πp) orbital overlap as a result of an increasing relativistic expansion[37] of the 4d and 5d orbitals and the absence of metal core/ligand repulsion proposed in first-row transition metal compounds.[38] The general trend of increasing N–M bond strength moving along the rows culminates in the highest observed M–N stretching frequency for NIrF$_3$. Unexpectedly, this trend does not apply to NFeF$_3$ which shows a lower M–N stretching frequency than the group 6 homologue (M=Cr). The lower stability of high-valent first row late transition metals is well known.[1a,39] In the series of 3d NM^{VI}F$_3$ compounds, for M=Fe it seems we have reached the limit of stability. NCo^{VI}F$_3$ is not a stable compound and only FNCoF$_2$ has been observed experimentally.[26] For the 4d element Rh it was found that the rearrangement of the

fluoro nitrene complex FNRhF$_2$ into N≡Rh^{VI}F$_3$ is only slightly exothermic ($\Delta H^0 = -12$ kJ mol^{-1}, CCSD(T)), which enables the observation of both rearrangement products.[26]

Within the atoms in molecules (AIM) scheme[40] the partial negative charge at the nitrido ligand in NMF$_3$ increases from M = Fe to Os (Tables S9 and S13), which indicates a decreasing electron withdrawing effect of the M^{VI}F$_3$ fragment within this group. For M=Fe and Ru the negative charge at the nitrogen atom also decreases from NMF$_2$ (M=Fe: −0.35, Ru: −0.40) to NMF$_3$ (M=Fe: −0.25, Ru: −0.35), while for M=Os it remains unchanged (NOsF$_2$: −0.50, NOsF$_3$: −0.49). As expected, fluorination of NMF$_3$ further decreases the atomic charge of the nitrido ligand in NMF$_4$ (M=Ru: −0.25, Os: −0.40, Table S9). The high oxidation potential of Fe^{VI} in NFeF$_3$ leads to relatively high σ^* and π^* occupation numbers (0.2 and 0.3 electrons, respectively; Figure S6). These indicates a weakened covalent N–Fe bond, for which the formal N^{3-} nitride notations seems to be a very poor approximation. The occupation of formally antibonding MOs also indicates an oxidation, and thus the onset of a redox non-innocent behavior of the nitrido ligand.

Conclusion

The nitrido complexes NFeF$_3$, NRuF$_3$, NRuF$_4$, NOsF$_3$ (^{1}A′), NOsF$_3$ (^{3}A″), and NOsF$_4$ were shown to be formed by the reaction of free group 8 metal atoms with NF$_3$ and established by their characteristic IR spectra recorded in solid neon matrices. Their assignment is supported by observed $^{14/15}$N isotope shifts and quantum-chemical predictions. All stretching fundamentals of the NM^{VI}F$_3$ complexes were confidently assigned. For the C_{4v} symmetric NRuF$_4$ two distinct bands were confidently assigned, whereas for NOsF$_4$ only the strongest band was tentatively assigned. Based on the joint experimental IR and quantum-chemical analysis the half-filled e^2 configuration of NFeF$_3$ can be assigned to an undistorted C_{3v} structure in a non-degenerate ^{3}A$_2$ electronic ground state. NFeF$_3$ features an unprecedented low Fe≡N triple-bond frequency of 946.7 (^{14}N≡Fe) and 922.7 cm^{-1} (^{15}N≡Fe). The heavier group 8 NMF$_3$ homologues are subject to symmetry lowering and spin-crossover caused by a pseudo Jahn–Teller effect "hidden" in the excited states. While the electronic ground state of NRuF$_3$ is a structurally distorted singlet ^{1}A′ state (C_s symmetry), for molecular NOsF$_3$ two coexisting distorted C_s structures with high-spin and low-spin d^2 configurations (magnetic bistability) were detected at 5 K in solid neon. To the best of our knowledge, apart from O$_2$Fe(η^2-O$_2$),[3–5] no other neutral Fe^{VI} complexes or molecular neutral complexes of Ru^{VII} have yet been reported, and after OsOF$_5$,[1f] NOsF$_4$ is the second known monomeric Os^{VII} compound.

Row	Group 4[a]	Group 6[b]	Group 8[c]	Group 9[d]	Group 11[30c]
3d	596.7 (Ti, C_{3v}, ^{3}A$_1$)	1015 (Cr, C_{3v}, ^{1}A$_1$)	946.4 (Fe, C_{3v}, ^{3}A$_2$)	FN=CoF$_2$ only	F$_2$N-CuF, FN=CuF$_2$
4d	553.1 (Zr, C_{3v}, ^{3}A$_1$)	1075 (Mo, C_{3v}, ^{1}A$_1$)	1098.5 (Ru, C_s, ^{1}A′)	1116.1 (Rh, C_s, ^{2}A′) [Ne] 1112.5 [Rh, Ar] [e]	F$_2$N–AgF only
5d	548.1 (Hf, C_{3v}, ^{3}A$_1$)	1091 (W, C_{3v}, ^{1}A$_1$)	1140.1 (Os, C_s, ^{1}A′) 1086.0 (Os, C_s, ^{3}A″)	1150.4 (Ir, C_s, ^{2}A′) [Ne] 1144.6 [Ir, Ar]	F$_2$N–AuF only

Table 2. Experimental M–N stretching frequencies [cm^{-1}] of NMF$_3$ molecules formed by the reaction of NF$_3$ with transition metals of group 4, 6, 8, 9, and 11.

[a] Ar matrix.[33] [b] Ar matrix.[25] [c] Ne matrix (this work). [d] Ne and Ar matrices.[26] [e] Formation of N≡RhF$_3$ along with FN=RhF$_2$.

Chemistry–A European Journal

Full Paper
doi.org/10.1002/chem.202101404

Chemistry Europe
European Chemical
Societies Publishing

Conflict of Interest

The authors declare no conflict of interest.

[1] a) S. Riedel, M. Kaupp, *Coord. Chem. Rev.* **2009**, *253*, 606–624; b) O. Ruff, E. Vidic, *Z. Anorg. Allg. Chem.* **1924**, *136*, 49–61; c) W. J. Casteel Jr, D. A. Dixon, H. P. A. Mercier, G. J. Schrobilgen, *Inorg. Chem.* **1996**, *35*, 4310–4322; d) A. O. Chong, K. Oshima, K. B. Sharpless, *J. Am. Chem. Soc.* **1977**, *99*, 3420–3426; e) K. Muniz, *Chem. Soc. Rev.* **2004**, *33*, 166–174; f) H. Shorafa, K. Seppelt, *Inorg. Chem.* **2006**, *45*, 7929–7934.
[2] H. Schmidbaur, *Z. Anorg. Allg. Chem.* **2018**, *644*, 536–559.
[3] Y. Gong, M. Zhou, L. Andrews, *J. Phys. Chem. A* **2007**, *111*, 12001–12006.
[4] W. Huang, D.-H. Xing, J.-B. Lu, B. Long, Schwarz, W. H. Eugen, J. Li, *J. Chem. Theory Comput.* **2016**, *12*, 1525–1533.
[5] J.-B. Lu, J. Jian, W. Huang, H. Lin, J. Li, M. Zhou, *Phys. Chem. Chem. Phys.* **2016**, *18*, 31125–31131.
[6] a) J. Hohenberger, K. Ray, K. Meyer, *Nat. Commun.* **2012**, *3*, 720; b) J. M. Smith, D. Subedi, *Dalton Trans.* **2012**, *41*, 1423–1429; c) B. Mondal, L. Roy, F. Neese, S. Ye, *Isr. J. Chem.* **2016**, *56*, 763–772.
[7] W. D. Wagner, K. Nakamoto, *J. Am. Chem. Soc.* **1988**, *110*, 4044–4045.
[8] J. F. Berry, E. Bill, E. Bothe, S. D. George, B. Mienert, F. Neese, K. Wieghardt, *Science* **2006**, *312*, 1937–1941.
[9] T. A. Betley, J. C. Peters, *J. Am. Chem. Soc.* **2004**, *126*, 6252–6254.
[10] J. L. Martinez, S. A. Lutz, H. Yang, J. Xie, J. Telser, B. M. Hoffman, V. Carta, M. Pink, Y. Losovyj, J. M. Smith, *Science* **2020**, *370*, 356–359.
[11] E. W. Svastits, J. H. Dawson, R. Breslow, S. H. Gellman, *J. Am. Chem. Soc.* **1985**, *107*, 6427–6428.
[12] a) T. Kandemir, M. E. Schuster, A. Senyshyn, M. Behrens, R. Schlögl, *Angew. Chem. Int. Ed.* **2013**, *52*, 12723–12726; *Angew. Chem.* **2013**, *125*, 12955–12959; b) G. Ertl, *Chem. Rec.* **2001**, *1*, 33–45.
[13] a) B. Askevold, J. T. Nieto, S. Tussupbayev, M. Diefenbach, E. Herdtweck, M. C. Holthausen, S. Schneider, *Nat. Chem.* **2011**, *3*, 532–537; b) B. M. Lindley, Q. J. Bruch, P. S. White, F. Hasanayn, A. J. M Miller, *J. Am. Chem. Soc.* **2017**, *139*, 5305–5308.
[14] a) W.-X. Ni, W.-L. Man, M. T.-W. Cheung, R. W.-Y. Sun, Y.-L. Shu, Y.-W. Lam, C.-M. Che, T.-C. Lau, *Chem. Commun.* **2011**, *47*, 2140–2142; b) W.-X. Ni, W.-L. Man, S.-M. Yiu, M. Ho, M. T.-W. Cheung, C.-C. Ko, C.-M. Che, Y.-W. Lam, T.-C. Lau, *Chem. Sci.* **2012**, *3*, 1582.
[15] K. Suntharalingam, T. C. Johnstone, P. M. Bruno, W. Lin, M. T. Hemann, S. J. Lippard, *J. Am. Chem. Soc.* **2013**, *135*, 14060–14063.
[16] K. Suntharalingam, W. Lin, T. C. Johnstone, P. M. Bruno, Y.-R. Zheng, M. T. Hemann, S. J. Lippard, *J. Am. Chem. Soc.* **2014**, *136*, 14413–14416.
[17] W.-X. Ni, W.-L. Man, W.-Q. Huang, C.-X. Wang, T. Liu, Z.-X. Li, C. Pan, Y.-Z. Chen, X. Lian, *Dalton Trans.* **2020**, *49*, 17173–17182.
[18] a) H.-X. Wang, L. Wu, B. Zheng, L. Du, W.-P. To, C.-H. Ko, D. L. Phillips, C.-M. Che, *Angew. Chem. Int. Ed.* **2021**, *60*, 4796–4803; *Angew. Chem.* **2021**, *133*, 4846–4853; b) N. B. Thompson, M. T. Green, J. C. Peters, *J. Am. Chem. Soc.* **2017**, *139*, 15312–15315; c) P. Vöhringer, *Dalton Trans.* **2020**, *49*, 256–266.
[19] a) J. J. Scepaniak, C. S. Vogel, M. M. Khusniyarov, F. W. Heinemann, K. Meyer, J. M. Smith, *Science* **2011**, *331*, 1049–1052; b) M. Keilwerth, L. Grunwald, W. Mao, F. W. Heinemann, J. Sutter, E. Bill, K. Meyer, *J. Am.*

[19] *Chem. Soc.* **2021**, *143*, 1458–1465; c) G. E. Cutsail, B. W. Stein, D. Subedi, J. M. Smith, M. L. Kirk, B. M. Hoffman, *J. Am. Chem. Soc.* **2014**, *136*, 12323–12336; d) G. Sabenya, L. Lázaro, I. Gamba, V. Martin-Diaconescu, E. Andris, T. Weyhermüller, F. Neese, J. Roithova, E. Bill, J. Lloret-Fillol, M. Costas, *J. Am. Chem. Soc.* **2017**, *139*, 9168–9177; e) L. Bucinsky, M. Breza, W.-T. Lee, A. K. Hickey, D. A. Dickie, I. Nieto, J. A. DeGayner, T. D. Harris, K. Meyer, J. Krzystek, A. Ozarowski, J. Nehrkorn, A. Schnegg, K. Holldack, R. H. Herber, J. Telser, J. M. Smith, *Inorg. Chem.* **2017**, *56*, 4752–4769.
[20] The "oxo wall" concept for terminal tetragonal oxo complexes is associated with d-orbital occupations beyond 5 and the resulting population of all metal-oxo pi* antibonding orbitals. Here, we refer to the concept of non-innocent ligands, which is of general importance in transition-metal chemistry and is not restricted to tetragonal complexes or to the occupation of antibonding MOs, but to the more general concepts of covalency and ligand field inversion. See ref. [22] and: L. Li, H. Beckers, T. Stüker, T. Lindič, T. Schlöder, D. Andrae, S. Riedel, *Inorg. Chem. Front.* **2021**, *8*, 1215–1228.
[21] a) W. Kaim, *Eur. J. Inorg. Chem.* **2012**, *2012*, 343–348; b) R. Hoffmann, S. Alvarez, C. Mealli, A. Falceto, T. J. Cahill, T. Zeng, G. Manca, *Chem. Rev.* **2016**, *116*, 8173–8192.
[22] N. Aliaga-Alcalde, S. DeBeer George, B. Mienert, E. Bill, K. Wieghardt, F. Neese, *Angew. Chem. Int. Ed.* **2005**, *44*, 2908–2912; *Angew. Chem.* **2005**, *117*, 2968–2972.
[23] M. P. Hendrich, W. Gunderson, R. K. Behan, M. T. Green, M. P. Mehn, T. A. Betley, C. C. Lu, J. C. Peters, *Proc. Natl. Acad. Sci. USA* **2006**, *103*, 17107–17112.
[24] a) J.-U. Rohde, T. A. Betley, T. A. Jackson, C. T. Saouma, J. C. Peters, Q. Lawrence Jr, *Inorg. Chem.* **2007**, *46*, 5720–5726; b) J. J. Scepaniak, M. D. Fulton, R. P. Bontchev, E. N. Duesler, M. L. Kirk, J. M. Smith, *J. Am. Chem. Soc.* **2008**, *130*, 10515–10517; c) C. Vogel, F. W. Heinemann, J. Sutter, C. Anthon, K. Meyer, *Angew. Chem. Int. Ed.* **2008**, *47*, 2681–2684; *Angew. Chem.* **2008**, *120*, 2721–2724.
[25] X. Wang, L. Andrews, R. Lindh, V. Veryazov, B. O. Roos, *J. Phys. Chem. A* **2008**, *112*, 8030–8037.
[26] T. Stüker, T. Hohmann, H. Beckers, S. Riedel, *Angew. Chem. Int. Ed.* **2020**, *59*, 23174–23179; *Angew. Chem.* **2020**, *132*, 23374–23379.
[27] a) P. Garcia-Fernandez, I. B. Bersuker, J. E. Boggs, *J. Chem. Phys.* **2006**, *125*, 104102; b) I. B. Bersuker, *Chem. Rev.* **2021**, *121*, 1463–1512.
[28] M. Laing, *J. Chem. Educ.* **1989**, *66*, 453.
[29] T. Schlöder, T. Vent-Schmidt, S. Riedel, *Angew. Chem. Int. Ed.* **2012**, *51*, 12063–12067; *Angew. Chem.* **2012**, *124*, 12229–12233.
[30] a) M. E. Jacox, *J. Phys. Chem. Ref. Data* **1998**, *27*, 115–393; b) D. E. Milligan, M. E. Jacox, *J. Chem. Phys.* **1964**, *40*, 2461–2466; c) Y. Gong, L. Andrews, *Inorg. Chem.* **2012**, *51*, 667–673.
[31] I. B. Bersuker, *Chem. Rev.* **2013**, *113*, 1351–1390.
[32] a) A. D. Becke, *Phys. Rev. A* **1988**, *38*, 3098–3100; b) J. P. Perdew, *Phys. Rev. B* **1986**, *33*, 8822–8824; c) F. Weigend, F. Furche, R. Ahlrichs, *J. Chem. Phys.* **2003**, *119*, 12753–12762; d) F. Weigend, R. Ahlrichs, *Phys. Chem. Chem. Phys.* **2005**, *7*, 3297–3305; e) D. Andrae, U. Huermann, M. Dolg, H. Stoll, H. Preu, *Theor. Chim. Acta* **1990**, *77*, 123–141.
[33] X. Wang, J. T. Lyon, L. Andrews, *Inorg. Chem.* **2009**, *48*, 6297–6302.
[34] P. Garcia-Fernandez, I. B. Bersuker, *Phys. Rev. Lett.* **2011**, *106*, 246406.
[35] B. O. Roos, A. C. Borin, L. Gagliardi, *Angew. Chem. Int. Ed.* **2007**, *46*, 1469–1472; *Angew. Chem.* **2007**, *119*, 1491–1494.
[36] P. Pyykkö, S. Riedel, M. Patzschke, *Chem. Eur. J.* **2005**, *11*, 3511–3520.
[37] P. Pyykkö, *Chem. Rev.* **1988**, *88*, 563–594.
[38] M. Kaupp, *J. Comput. Chem.* **2007**, *28*, 320–325.
[39] S. X. Hu, W. L. Li, J. B. Lu, J. L. Bao, H. S. Yu, D. G. Truhlar, J. K. Gibson, J. Marçalo, M. Zhou, S. Riedel, Schwarz, W. H. Eugen, J. Li, *Angew. Chem. Int. Ed.* **2018**, *57*, 3242–3245; *Angew. Chem.* **2018**, *130*, 3297–3300.
[40] R. F. W. Bader, *Atoms in Molecules: A Quantum Theory*, Clarendon, Oxford, **1994**.
[41] L. Bennett, B. Melchers, B. Proppe, *Curta: A General-Purpose High-Performance Computer at ZEDAT, Freie Universität Berlin;* Freie Universität Berlin, **2020**.